Vol 13 No 9, September 2004
1009-1963/2004/13(09)/1526-05

Chinese Physics

© 2004 Chin. Phys. Soc.
and IOP Publishing Ltd

Phonon spectrum of single-walled boron nitride nanotubes*

Xiao Yang(肖 杨)[a], Yan Xiao-Hong(颜晓红)[a,b]†, Cao Jue-Xian(曹觉先)[a,b], Mao Yu-Liang(毛宇亮)[a], and Xiang Jun(向 君)[a]

[a] *Department of Physics & Institute of Modern Physics, Xiangtan University, Xiangtan* 411105, *China*
[b] *Interdisciplinary Center of Theoretical Studies and Institute of Theoretical Physics, Chinese Academy of Sciences, Beijing* 100080, *China*

(Received 2 December 2003; revised manuscript received 29 April 2004)

Based on a force constant model, we investigated the phonon spectrum and then specific heat of single-walled boron nitride nanotubes. The results show that the frequencies of Raman and infrared active modes decrease with increasing diameter in the low frequency, which is consistent with the results calculated by density functional theory. The fitting formulae for diameter and chirality dependence of specific heat at 300K are given.

Keywords: phonon spectrum, nanotube, boron nitride
PACC: 6320D, 6322

1. Introduction

Following the discovery[1] and extensive research[2−6] of carbon nanotube (CNT), its derivative boron nitride nanotubes (BNNTs) have attracted considerable attention in recent years due to anticipated exciting properties. It is found that BNNTs have exceptional mechanical properties. For example, the axial Young modulus of multi-walled BNNTs has been measured to be 1.22×10^{12}Pa.[7] Contrary to the bandstructures dependent on the geometrical structures of CNTs,[8] however, in BNNTs there exists an energy gap of 5eV,[9−11] which is independent of the number of walls, diameter, or chirality. Such a wide energy gap implies potential applications of BNNTs in nanosized electronic devices. In these nanoelectronic applications, excellent thermal properties, such as thermal conductivity, are indispensable.

It is an effective avenue to investigate phonon structure for the study of thermal properties of BNNTs. A series of calculations of phonons in BNNTs have been performed using density functional theory (DFT),[12,13] and the valence shell model.[14] Of these, the valence shell model provides a good understanding of phonons based on force constants fitting the phonon dispersion of a monolayer of hexagonal boron nitride (h-BN).[15] However, the quadratic wavevector dependence of the frequency of out-of-plane phonons cannot be produced using two-body interaction force constants.[14] Reasonable phonon dispersion relations (PDRs) of 2D h-BN and BNNTs could be obtained by virtue of DFT calculations. Nevertheless, the large computational demand restricts the application to large-diameter nanotubes, especially to chiral nanotubes. Here we present calculations of phonons in BNNTs with a force constant model, which has been used to study phonons in CNTs.[16,17] In order to study phonon spectra of chiral BNNTs with a large number of atoms in the unit cell, we can reduce the unit cell to a two-atom cell based on the symmetry of nanotubes.[18−20] The symmetry reduces the dimension of dynamical matrix to six, independent of the number of atoms in the unit cell. Consequently, this method can be applied conveniently to the calculations of phonon spectrums in chiral BNNTs.

*Project supported by Science and Technology Foundation for Ministry of Education (Grant No 204099) and by the Science and Technology Foundation for Education Bureau of Hunan Province (Grant No 03A046), and partly by the Natural Science Foundation of Hunan Province (Grant Nos 03JJY3010 and 03JZY3019).
†Email address: xhyan@xtu.edu.cn

2. Model and parameters

The PDRs of 2D h-BN and BNNTs are calculated with the force constant model. In this model, it is crucial to determine the force constants between two atoms. Due to the nature of layer-structure in h-BN, a nearly quadratic wave-vector dependence of frequency of out-of-plane phonons is expected.[21] However, force constant parameters up to the second nearest neighbours cannot reproduce the quadratic dependence.[14] Accordingly, we introduce 15 force constant parameters to describe the dependence of out-of-plane phonons. The best-fit parameters are given in Table 1, in which $\phi_{\rm r}$, $\phi_{\rm ti}$ and $\phi_{\rm to}$ represent the force constant in the radial, in-plane and out-of-plane tangential directions, respectively.[22]

Table 1. Force constant parameters for 2D h-BN in units of N/m. The subscripts r, ti, and to refer to radial, transverse in-plane and transverse out-of-plane, respectively.

Radial	Tangential	
$\phi_{\rm r}^{(1)} = 310$	$\phi_{\rm ti}^{(1)} = 185$	$\phi_{\rm to}^{(1)} = 56$
$\phi_{\rm r}^{(B-B)} = 70$	$\phi_{\rm ti}^{(B-B)} = -32.3$	$\phi_{\rm to}^{(B-B)} = -7.0$
$\phi_{\rm r}^{(N-N)} = 80$	$\phi_{\rm ti}^{(N-N)} = -7.3$	$\phi_{\rm to}^{(N-N)} = -5.5$
$\phi_{\rm r}^{(3)} = 10$	$\phi_{\rm ti}^{(3)} = -32.5$	$\phi_{\rm to}^{(3)} = 6.5$
$\phi_{\rm r}^{(4)} = -19$	$\phi_{\rm ti}^{(4)} = 12.9$	$\phi_{\rm to}^{(4)} = -3.0$

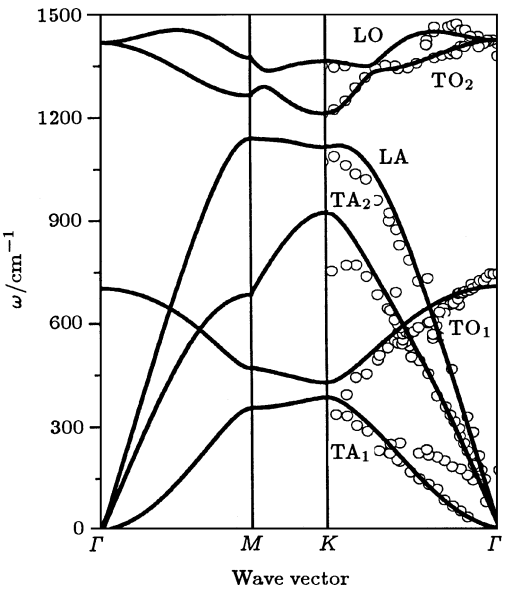


Fig.1. Phonon dispersion relation of 2D h-BN. The circles represent the experimental data from Ref.[15].

Using the force constant parameters in Table 1, the PDRs of 2D h-BN, frequency–wave vector curve are calculated as shown in Fig.1, in which the available measured points are included for comparison. The out-of-plane acoustic and optical phonon branches are denoted by TA_1 and TO_1, while in-plane acoustic and optical phonon branches are denoted by TA_2, LA, TO_2, and LO, respectively. It is noted that the optical branches with a flat dispersion curve around 160cm^{-1} in the experimental points are not well described by the present calculations. This condition is believed to hold in our case, judging from the fact that in this optical mode the whole h-BN overlayer vibrates against the substrate at Γ.[15] Compared with experimental data and the DFT results,[13] the current calculations are more precise than those presented in Ref.[14]. These results indicate that the method presented is reasonable and that the parameters listed in Table 1 are reliable.

3. Results and analysis

With the force constant model and parameters mentioned above, the phonon modes of BNNTs are obtained. As a typical example, we calculate the PDRs of (10, 10) and (17, 0) BNNTs as shown in Fig.2. One can see that there are only 66 and 108 distinct branches, in which 12 modes are nondegenerate and the other are doubly degenerate. These results are consistent with the analysis of rod group of BNNTs.[23] As presented by Alon, the rod groups for zigzag $(n, 0)$, armchair (n, n) and (n, m) chiral BNNTs are respectively C_{2nv}, C_{2nh} and C_N, where $N = 2(n^2 + m^2 + nm)/d_{\rm R}$ with $d_{\rm R}$ being the great common divisor of $2n + m$ and $2m + n$. Around Γ point, there are four acoustic modes: two degenerate transverses (TA), one twisting (WA), and one longitudinal (LA), all of which have linear dispersions at low energy. The sound velocities of the TA, WA and LA modes for a (10, 10) BNNT are estimated as 8.73, 12.85 and 17.17km/s, respectively. The high sound velocity and the small diameter cause the relatively large subband splitting. Such a splitting would have an important effect on specific heat.

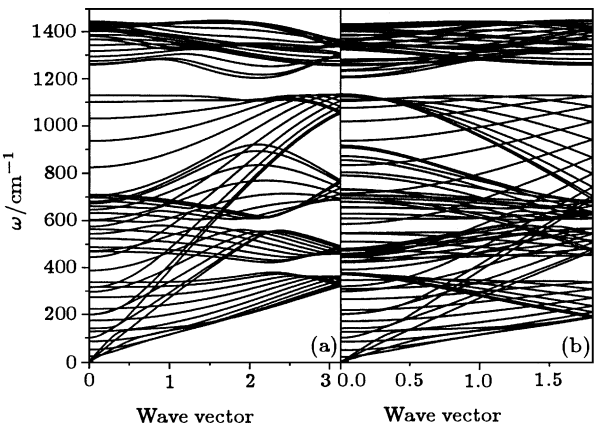


Fig.2. Phonon dispersion relation of BNNTs in the direction of the tube axis. (a) For (10, 10) PDR and (b) for (17, 0) BNNT.

In Fig.3, we plot the frequencies of the Raman and infrared (IR) active modes for zigzag, chiral and armchair BNNTs as functions of diameter. Based on the rod group,[23] the Raman and IR active phonon modes are assigned as follows:

$$\Gamma_{\text{Raman}}^{\text{arm}} = 3A_{\text{g}} \oplus 2E_{1\text{g}} \oplus 4E_{2\text{g}},$$
$$\Gamma_{\text{IR}}^{\text{arm}} = A_{\text{u}} \oplus 3E_{1\text{u}}, \quad (1)$$
$$\Gamma_{\text{Raman}}^{\text{zig}} = 3A_1 \oplus 5E_1 \oplus 6E_2,$$
$$\Gamma_{\text{IR}}^{\text{zig}} = 3A_1 \oplus 5E_1, \quad (2)$$
$$\Gamma_{\text{Raman}}^{\text{ch}} = 4A \oplus 5E_1 \oplus 6E_2,$$
$$\Gamma_{\text{IR}}^{\text{ch}} = 4A \oplus 5E_1. \quad (3)$$

From the relations (1), (2), (3), one can see that the set of IR modes is a subset of the Raman modes for zigzag and chiral BNNTs, while the set of IR modes and Raman modes is separated for armchair tubes. The modes in Fig.3 can be divided into three frequency regimes: low frequency ($\omega < 600\text{cm}^{-1}$), medium frequency around 700cm^{-1}, and high frequency near 1400cm^{-1}. In the high and medium frequencies, the frequencies of modes are insensitive to diameter for large diameter BNNTs. However, in the low frequency, the frequency of modes decreases rapidly with increasing diameter and approaches zero for $d \to \infty$. In addition, the low frequency modes display a simple power law as $\omega \propto 1/d^n$, with n=2 for the lowest mode, while n=1 for the other modes. This scaling relation is in agreement with that calculated by the DFT method.[13]

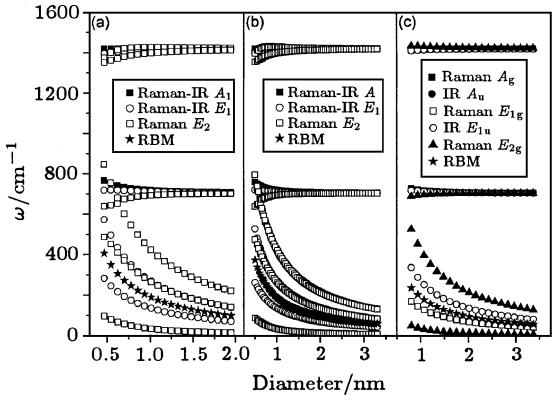


Fig.3. Raman and IR active modes in BNNTs as a function of diameter. (a) For zigzag BNNT, (b) for chiral BNNT and (c) for armchair BNNT.

The radial breathing modes (RBM) are known to have strong Raman intensities in the low frequency, and can be used to characterize the CNTs samples.[24,25] It is easily found that the frequency of RBM (marked by an asterisk in Fig.3) decreases with increasing diameter and is inversely proportional to the diameter. The numerical fitting can lead to the inverse dependence formula

$$\omega_{\text{RBM}} = A/r, \quad (4)$$

where r is radius of BNNTs and A=9.51 $\times$ $10^{-8}\text{cm}^{-1}\cdot\text{m}$. The value of A is consistent with the value of $1.005 \times 10^{-7}\text{cm}^{-1}\cdot\text{m}$[12] and $1.03 \times 10^{-7}\text{cm}^{-1}\cdot\text{m}$[13,26] by DFT calculations, while larger than that of $8.51 \times 10^{-8}\text{cm}^{-1}\cdot\text{m}$ proposed by Popov.[14]

As the PDR is determined, the vibrational density of states (VDOS) can be written as

$$g(\omega) = \frac{\Omega}{(2\pi)^3}\int \frac{\text{d}S}{|\nabla_q \omega(q)|} = \frac{\Omega}{(2\pi)^3}\sum_q \frac{\delta}{(\omega-\omega_q)^2+\delta^2}, \quad (5)$$

where δ is an adjustable width factor of Lorentzian function. In terms of VDOS, the specific heat C_{V} at temperature T is given by the formula

$$C_{\text{V}}(T) = \int_0^{\omega_{\max}} k_{\text{B}} \left(\frac{\hbar\omega}{k_{\text{B}}T}\right)^2 \times \frac{\exp(\hbar\omega/k_{\text{B}}T)}{[\exp(\hbar\omega/k_{\text{B}}T)-1]^2} g(\omega)\text{d}\omega, \quad (6)$$

where $\hbar$ and k_{B} are the Planck constant and the Boltzmann constant, respectively. The calculated specific heat and VDOS of (10, 10) BNNT are shown in Fig.4, together with a comparison with those of (10, 10) CNT. Below 6K, the specific heat of BNNTs increases linearly with increasing temperature (see the inset of Fig.4 (a)), and displays a temperature dependence similar to that of CNTs. This behaviour is attributed to the constant VDOS at low energy in Fig.4 (b). Above 6K, the slope of the specific heat increases due to the populations of optical subbands, which is expected to be the signature of 1D quantized phonon spectrum in single-walled BNNTs. An analogous situation is found for (10, 10) CNTs. The periodic boundary condition on the circumferential wavevector splits phonon modes into 1D van Hove singularities in the VDOS in Fig.4(b). Because the phonon contribution to specific heat is determined by the VDOS, the van Hove singularities in VDOS would have an important influence on specific heat. At low energy, BNNT has a larger value of VDOS than CNT, which leads to a difference in specific heat between BNNT and CNT. In Fig.4(a), the curve of (10, 10) BNNT lies well above that of (10, 10) CNT. This fact indicates that CNTs maybe have a higher thermal conductivity than BNNTs. At low temperature, the Umklapp scattering

freezes out and phonon mean free path l is constant with temperature.[27–29] Therefore, the phonon thermal conductivity follows the temperature dependence of specific heat. Assuming BNNT has the same l as CNT, BNNT would have a larger low-temperature thermal conductivity than CNT. An accurate measurement of thermal conductivity of BNNTs, as well as modelling theoretically, would help clarify this issue.

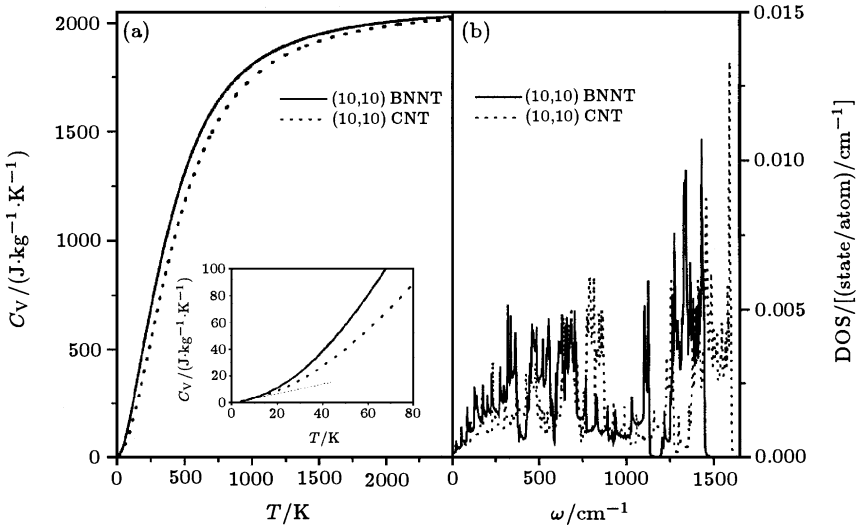


Fig.4. (a) Specific heat (b) vibrational density of state of (10, 10) BNNT and CNT.

The diameter and chirality dependence of specific heat at 300K for 330 BNNTs (n=6–25, $m = 0 - n$) are shown in Fig.5. It is found that specific heat increases with increasing diameter and approaches the $C_{V2D} = 841\,J\cdot kg^{-1}\cdot K^{-1}$ (C_{V2D} is specific heat of 2D h-BN at 300K) (see Fig.5(a)). From the inset, one can see that specific heat is linear with d^{-2} with the diameter d. The best-fit formula is given by

$$C_V(T) = C_{V2D} - 7.6/d^2. \tag{7}$$

This fitting is in agreement with calculated results for large diameter BNNTs, while has a deviation for small diameter BNNTs. The deviation may be attributed to the curvature effect of small diameter nanotubes. The chirality dependence of specific heat is shown in Fig.5(b). The specific heat increases with tube indices for small diameter BNNTs, while it is insensitive to tube indices for large diameter BNNTs. It is easy to fit specific heat at 300K in (n, m) BNNT by

$$C_V = C_{V2D} - \frac{B}{d^2}\left[240.0 + 57.3\arctan\left(\frac{\sqrt{3}m}{2n+m}\right)\right] \tag{8}$$

with $B = 0.03\,J\cdot kg^{-1}\cdot K^{-1}\cdot nm^2/(^\circ)$. Due to the chiral angle $\theta = 57.3\arctan\left(\frac{\sqrt{3}m}{2n+m}\right)$ (degree), Eq.(8) is simplified to $C_V = C_{V2D} - \frac{B}{d^2}[240.0 + \theta]$. The presented formula takes into account the essential relation between the specific heat and tube indices (n, m) and can be used for the qualitative evaluation in relatively wide tube indices/diameter range.

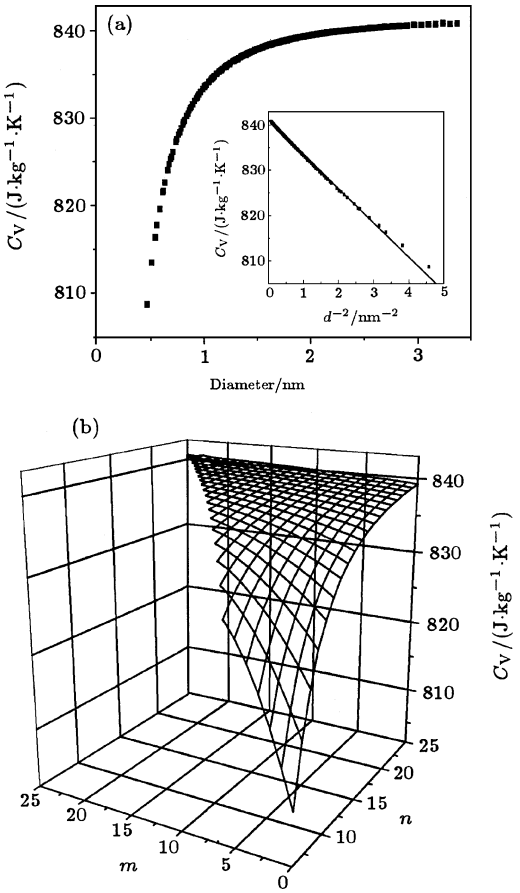


Fig.5. (a) Specific heat of BNNTs at 300K as a function of the tube diameter (b) the tube indices.

4. Conclusion

We have investigated the PDRs, VDOS, and specific heat of BNNTs based on a force constant model within lattice dynamics theory. The dynamical matrix of BNNTs is obtained directly using the force constant parameters, which are determined by fitting the measured data. It is found that PDRs of BNNTs have a series of subbands and high sound velocities at Γ. Assignment of Raman and IR active modes has shown that low frequency modes are more sensitive to diameter than high frequency modes. Moreover, the specific heat of BNNTs displays a linear temperature dependence at low temperature, while BNNTs have a larger specific heat due to larger VDOS. Using phonon spectra, the diameter and chiral angle dependence of specific heat at 300K are calculated. The best-fitting formulae of all types of BNNTs for diameter and chirality dependence are $C_{\rm V}(T) = C_{\rm V2D} - 7.6/d^2$ and $C_{\rm V} = C_{\rm V2D} - \dfrac{B}{d^2}\left[240.0 + 57.3\arctan\left(\dfrac{\sqrt{3}m}{2n+m}\right)\right]$, respectively.

References

[1] Iijima S 1991 *Nature* **354** 56

[2] Peng L M, Zhang Z L, Xue Z Q, Wu Q D, Gu Z N and Pettifor D G 2000 *Phys. Rev. Lett.* **85** 3249

[3] Fan S S, Michael C, Thomas T, Cassell A and Dai H J 1999 *Science* **283** 512

[4] Sun J P and Wang T H 2002 *Acta Phys. Sin.* **51** 2096 (in Chinese)

[5] Sun L F, Xie S S, Liu W, Zhou W Y, Liu Z Q, Tang D S, Wang G and Qian L X 2000 *Nature* **403** 384

[6] Xiao Y, Yan X H, Cao J X and Ding J W 2003 *J. Phys.: Condens. Matter* **15** L341

[7] Chopra N G and Zettl A 1998 *Solid State Commun.* **105** 297

[8] Ding J W, Yan X H and Cao J X 2002 *Phys. Rev.* B **66** 073401

[9] Zhang Z H, Peng J C and Zhang H 2001 *Appl. Phys. Lett.* **79** 3515

[10] Rubio A, Corkill J L and Cohen M L 1994 *Phys. Rev.* B **49** 5081

[11] Blase X, Rubio A, Louie S G and Cohen M L 1994 *Europhys. Lett.* **28** 3085

[12] Xiang H J, Yang J L, Hou J G and Zhu Q S 2003 *Phys. Rev.* B **68** 035427

[13] Wirtz L, Rubio A, Arenal de la Concha R and Loiseau A 2003 *Phys. Rev.* B **68** 045425

[14] Popov V N 2003 *Phys. Rev.* B **67** 085408

[15] Rokuta E, Hasegawa Y, Suzuki K, Gamou Y, Oshima C and Nagashima A 1997 *Phys. Rev. Lett.* **79** 4609

[16] Saito R, Takeya T, Kimura T, Dresselhaus G and Dresselhaus M S 1998 *Phys. Rev.* B **57** 4145

[17] Cao J X, Yan X H, Xiao Y, Tang Y and Ding J W 2003 *Phys. Rev.* B **67** 045413

[18] Cao J X, Yan X H, Xiao Y 2003 *J. Phys. Soc. Jpn.* **72** 2256

[19] Xiao Y, Yan X H, Cao J X and Ding J W 2003 *Acta. Phys. Sin.* **52** 1720 (in Chinese)

[20] Maultzsch J, Reich S, Thomsen C, Dobardzic E, Milosevic I and Damnjanovic M 2002 *Solid State Commun.* **121** 471

[21] Jishi R A and Dresselhaus G 1982 *Phys. Rev.* B **26** 4514

[22] Jishi R A, Venkataraman L, Dresselhaus G and Dresselhaus M S 1993 *Chem. Phys. Lett.* **209** 77

[23] Alon O E 2001 *Phys. Rev.* B **64** 153408

[24] Lu J Q, Wu J, Duan W, Liu F, Zhu B F and Gu B L 2003 *Phys. Rev. Lett.* **90** 156601

[25] Wang Y F, Cao X W, Hu S F, Liu Y Y and Lan G X 2001 *Chem. Phys. Lett.* **336** 47

[26] Akdim R, Pachter R, Duan X F and Adams W W 2003 *Phys. Rev.* B **67** 245404

[27] Hone J, Whitney M, Piskoti C and Zettl A 1999 *Phys. Rev.* B **59** R2514

[28] Yi W, Lu L, Zhang D L, Pan Z W and Xie S S 1999 *Phys. Rev.* B **59** R9015

[29] Kim P, Shi L, Majumdar A and McEuen P L 2001 *Phys. Rev. Lett.* 87 215502